DIAPHRAGM SEALING STRATEGIES FOR MEMS LOUDSPEAKERS

Nils Wittek[1,2], Anton Melnikov[2], André Zimmermann[1,3]

[1] *University of Stuttgart, Institute for Micro Integration (IFM), 70569 Stuttgart, Germany*
[2] *Bosch Sensortec GmbH, Robert-Bosch-Ring 1, 01109 Dresden, Germany*
[3] *Hahn-Schickard, 70569 Stuttgart, Germany*

This paper is a revised version of the authors' submitted manuscript that was peer-reviewed by at least two anonymous reviewers.

Abstract

This paper presents a comparative analysis of diaphragm sealing strategies for piezoelectric MEMS loudspeakers, focusing on their impact on sound pressure level (SPL) across the audible frequency range. Effects on actuator design, manufacturing complexity, and reliability are also evaluated. An analytical model is introduced to estimate acoustic leakage, along with a new criterion for defining leakage.

Keywords: *MEMS, speaker, sealing, piezoelectric, diaphragm.*

1. Introduction

Following the success of MEMS microphones, MEMS speakers are attracting increased research interest. Especially speakers based on the piezoelectric transduction principle are investigated due to a favorable ratio between required driving voltage and diaphragm displacement [1]. Piezoelectric MEMS speakers were first built with a fully clamped diaphragm leading to high stiffness and therefore lower displacement under a given driving voltage, especially considering the small sizes of MEMS speakers [1], [2]. Using cantilever structures configured as unimorphs or bimorphs, which incorporate one or two piezoelectric actuators respectively, allows for greater displacement under the same applied voltage [1], [3]. These actuators are based on cantilever structures, which can be designed with either free ends or a central connecting mass to enable piston-like movement and are widely represented in current scientific literature [3], [4]. An inherent downside of using cantilevers is the loss of sound pressure level (SPL) due to leakage especially at low frequencies where viscous boundary layers can't be used to acoustically seal the device [5]. Different approaches have been taken to provide acoustic sealing also at low frequencies with Parylene-C and PDMS as primary candidates [6], [7]. While a systematic comparison of sealing strategies remains unreported, leakage could also play a role in emerging ultrasound pulse-based MEMS speakers, as their small features and high operating frequencies may influence the leakage behavior [8].

Corresponding author: *nils.wittek@ifm.uni-stuttgart.de.*

2. Sealing Strategies for MEMS Speakers

Three sealing strategies are investigated: (1) mechanical slit reduction relying on viscous boundary layers, following the mechanically-open and acoustically-closed (MOAC) approach; (2) complete slit sealing with stretchable films; and (3) selective slit sealing with stretchable films. Considered flexible sealing materials are Parylene-C and PDMS. The presented measurement data are analyzed regarding the influence on performance and manufacturability. This enables a comparison between the different sealing strategies and associated materials, providing an overview of their suitability across different application areas and frequency ranges.

The following sections present the different approaches to diaphragm sealing, with consideration of material choices.

2.1. MOAC

The MOAC approach is based on structures with narrow slits between mechanical elements [1], [4], [5], [9], [10]. These slits allow greater mechanical deflection compared to fully clamped diaphragms [9], while viscous boundary layers suppress acoustic leakage, effectively decoupling front and back volume [1]. Slit airflow is governed by geometry, vibration frequency, and pressure difference between diaphragm sides. At the interface of structure to air, zero velocity at boundaries induces high viscous losses [5]. As the slit width increases, the relative influence of these viscous losses decreases, allowing for a higher acoustic particle velocity within the slit. Although higher frequencies reduce boundary layer thickness and increase slit velocity [4], [9], leakage remains low due to limited time for pressure equalization [4]. At frequencies below 1 kHz, wider slits compromise sealing and cause significant pressure loss [4].

Simulations and experiments confirm that slit widths of 5 µm or less minimize leakage and preserve flow behavior when paired with a sufficiently large back volume [1], [4], [5], [9], [10]. Larger slits increase average velocity and parasitic airflow [5]. Sound pressure level (SPL) rises with smaller slits at low frequencies due to the reduced acoustic leakage [5].

Uniform slit dimensions are critical but can vary due to large displacements from high voltages or deflection from residual stress release [5]. This can be mitigated by central coupling structures in triangular cantilevers [1] or acoustic shields that maintain slit geometry during actuation, suitable for asymmetric cantilever designs [4].

The primary fabrication challenge is achieving narrow slits, with 3 µm being the current minimum [4]. Once realized, the absence of a sealing diaphragm enhances acoustic performance and efficiency, as energy is not stored in elastic structural elements [4]. It also simplifies manufacturing by eliminating the need for additional sealing layers [9].

A comparison of achieved slit widths is provided in Tab. 1, showing that slit widths range from 3 µm to 10 µm.

2.2. Complete Sealing

2.2.1. Parylene-C

Parylene-C is a commonly used flexible sealing layer to prevent air leakage in diaphragm structures using cantilevers divided by slits [2], [6], [11], [15], [16]. Its material properties are summarized in Table 2. Sealing the entire diaphragm increases its mass, which lowers the resonance frequency according to $\omega = \sqrt{\frac{k}{m}}$, where k is stiffness and m is mass. This effect has to be considered in the design process. While layer thickness has minimal impact on sound pressure level (SPL), thinner layers lead to a slightly better performance [2]. Although leakage is effectively suppressed, overall SPL remains lower than in cantilever diaphragms without sealing layers.

In some studies, Parylene-C is deposited before diaphragm release, which restricts cantilever deformation and limits residual stress relaxation [2], [6]. This can increase stiffness and reduce sensitivity [13], possibly explaining the higher resonance frequency and lower SPL observed in [6]. In contrast, a 0.5 µm thin layer that is suspended over the slits was used in [2], allowing greater deflection and enhancing displaced volume through the Parylene-C layer in the slits. However, this design may suffer from layer separation during continuous operation, as reported in [12].

Durability of Parylene-C can be a concern, as observed pinholes and cracks can cause leakage and reduce chamber pressure, lowering SPL [6]. Scratches on the electrode area observed in [16] likely result from friction during vibration, while long-term operation at 100 V_{pp} has led to scratches and bubbles in the coupling structure, suggesting embrittlement due to high-voltage excitation [16].

Despite these issues, Parylene-C offers protective benefits. It prevents diaphragm rupture and blocks dust and liquids from entering the slits [6]. It also relieves stress and buffers mechanical strain at slit edges, preventing mechanical damage under high-voltage actuation [15], [16].

A comparison in Tab. 1 shows sealing layer heights between 0.5 µm to 6 µm, and sealed slit widths from 4.3 µm to 10 µm.

2.2.2. PDMS

Another solution to the acoustic short-circuit issue in piezoelectric MEMS speakers involves sealing the slits between actuators after diaphragm release using a stretchable film of polydimethylsiloxane (PDMS) covering the entire diaphragm. During actuation, the film primarily undergoes tensile deformation. To minimize constraints on diaphragm bending, the sealing layer must exhibit high tensile compliance. [7]

Compared to Parylene-C, PDMS enables higher sensitivity and preserves the resonance frequency due to its significantly lower Young's modulus, as shown in Tab. 2. This simplifies both design and fabrication, as no additional structuring is required. [7]

Simulations show that PDMS sealing flattens the low-frequency SPL response while maintaining the original sensitivity. Experimental results confirm this behavior. After sealing, the low-frequency performance improves significantly, with SPL above 250 Hz remaining largely unaffected. The resonance frequency decreases by less than 1 kHz, probably due to the added mass of the PDMS film, indicating that high-frequency performance is preserved. [7]

PDMS also demonstrates thermal stability. Acoustic performance remains consistent before and after 260 °C heat treatment, confirming compatibility with standard reflow processes [7].

Tab. 1 lists the only reported example of this approach, where a 15 µm PDMS layer seals slit widths of 14 µm.

2.3. Selective Sealing

Selective sealing with stretchable film materials can be used to either seal only the region of the slits, parts of the slits, or the diaphragm structure besides the slits.

2.3.1. Parylene-C

The only reported design with selective Parylene-C sealing is presented in [12], as an enhancement of the earlier approach in [2]. In this design, a thicker Parylene-C layer is applied exclusively to the diaphragms, leaving the slits uncovered. However, the film partially extends into the slit sidewalls, effectively narrowing them. Therefore, this configuration leverages the MOAC principle to suppress acoustic leakage. The Parylene-C layer primarily reduces slit

Table 1: Comparison of MEMS speakers using different sealing strategies, ordered by publication date.

Article	Sealing Strategy	Sealing Material	Slit Width [µm]	Height Sealing Layer [µm]
Stoppel [5]	MOAC	-	4	-
Stoppel [9]	MOAC	-	9	-
Wang [2]	Complete	Parylene-C	9	0.5
Gazzola [1]	MOAC	-	10	-
Ma [6]	Complete	Parylene-C	10.35	6
Xu [7]	Complete	PDMS	14[a]	15
Deng [11]	Complete	Parylene-C	4.3	3.5
Wang [12]	Selective	Parylene-C	9	0.5
Wang [13]	Selective	PDMS	6.8	-
Cerini [10]	MOAC	-	5	-
Chen [14]	Selective	PDMS	6.82	-
Stoppel [4]	MOAC	-	3	-
Zheng [15]	Complete	Parylene-C	10	2.3
Zheng [16]	Complete	Parylene-C	10	2.3

[a]Not explicitly stated, estimated from images.

Table 2: Sealing material properties from [13], compared to silicon for reference [17].

Materials	Density [$\mathrm{kg\,m^{-3}}$]	Young's Modulus [GPa]	Tensile Strength [MPa]
PDMS	970	$0.75 \cdot 10^{-3}$	6.9
Parylene-C	1289	2.76	69
Silicon	2929	130...188	500...1000

sizes and improves mechanical stability under large displacements and high voltages.

Slit width and sealing layer thickness for this device are given in Tab. 1, with a sealing layer of 0.5 µm applied to slits of 9 µm width.

2.3.2. PDMS

A strategy for selective sealing is presented in [13], where only the slits of a cantilever diaphragm are sealed with PDMS. The sealing is applied post-release, with capillary forces guiding the liquid PDMS through the slits, followed by a curing step. This self-driven process simplifies application and reduces equipment requirements.

Due to its low Young's modulus and high elasticity, cured PDMS has minimal impact on the mechanical behavior of the diaphragm, especially when compared to stiffer materials like Parylene-C, as shown in Tab. 2. Sealing the slits significantly improves SPL below 100 Hz by preventing acoustic short circuits.

Connecting the individual cantilever elements of the diaphragm also leads to a uniform resonance frequency of the device, as through manufacturing tolerances, all cantilevers have a slightly different resonance frequency. By connecting them through the sealing material, a single resonance frequency of the entire diaphragm is achieved, improving SPL around the resonances, as cancellation of individual cantilevers due to phase shifts is prevented.

Fractures of the PDMS inside the slits were not observed. Performance of the speaker only reduced slightly while operated continuously for several days. The material also remains stable across a wide temperature range from −45 °C to 200 °C.

The same method of sealing is used in [14], where only the slits and etching holes at the clamped edges are sealed. While this improves low-frequency response, some SPL loss remains, likely due to incomplete sealing.

The two reported designs are listed in Tab. 1, with slit widths of 6.8 µm and no specified sealing layer height.

3. Modeling of the MOAC Approach

The MOAC approach is advantageous because it does not require an additional sealing layer, provided that sufficiently small slit widths are achieved. To assess the validity of the recommended minimum gap size of 5 µm, an analytical model describing acoustic leakage is developed, together with a criterion for the onset of leakage. The model is then evaluated using FEM simulations.

3.1. Boundary Layer Thickness

According to [18], the viscous boundary layer thickness above a flat plate in air is given by Eq. (1), where η is the viscosity of air, ω the angular frequency, and ρ_0 the equilibrium density.

$$\delta_\mathrm{v} = \sqrt{\frac{2\eta}{\omega\rho_0}} \tag{1}$$

For a slit, the boundary layer thickness is doubled to account for both sides. In the audible frequency range, the boundary layers typically exceed 30 µm, which should be sufficient to prevent flow. However, at low frequencies, the longer pressure equalization times allow air to still pass through the slits. Therefore, another approach is needed to estimate leakage analytically.

3.2. Analytical Model for Leakage Estimation

A diaphragm compressing air in a cavity with slits can be described using an equivalent circuit as shown in Fig. 1, where volume flow is analogous to current and pressure to voltage. The moving diaphragm acts as a frequency-dependent current source Q_{in}, injecting volume flow into the cavity. The cavity is modeled by the capacitance C_{cavity}, which represents the ear volume, and the resulting cavity pressure is denoted by p_{cavity}. Leakage through the side slits is modeled as a resistance R_{slit}.

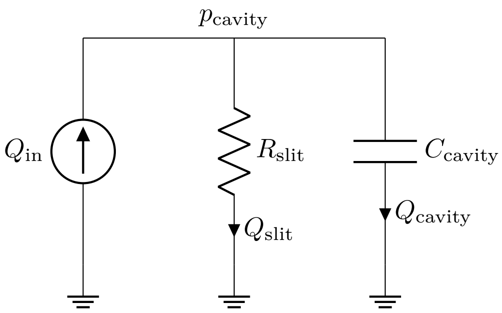

Figure 1: Equivalent circuit for describing leakage.

The slit resistance R_{slit} and cavity capacitance C_{cavity} are represented as lumped elements [19]. The relevant equations are given in (2) and (3). Here, $\eta = 1.81 \times 10^{-5}$ Pa s is the dynamic viscosity of air, l the slit length, b the slit depth, and d the slit width. For the capacitance, $V_0 = 1.26 \times 10^{-6}\,\text{m}^3$ is the standardized ear coupler volume according to IEC 60318-4, $\kappa = 1.4$ the specific heat ratio of air, and $p_0 = 101\,325$ Pa the ambient pressure. This model neglects air inertia in the slit due to the small volume and assumes adiabatic conditions without heat exchange.

$$R_{\text{slit}} = \frac{12 \cdot \eta \cdot l}{b \cdot d^3} \tag{2}$$

$$C_{\text{cavity}} = \frac{V_0}{\kappa \cdot p_0} \tag{3}$$

The equation for the slit resistance (2) is valid up to the characteristic frequency f_0, defined in Eq. (4). Above this frequency, the boundary layers no longer cover the entire slit and the resistance becomes frequency dependent [19].

$$f_0 = \frac{36 \cdot \eta}{\pi \cdot \rho_0 \cdot d^2} \tag{4}$$

This system behaves as a high-pass filter, with the transfer function given in Eq. (5). The ratio of R_{slit} to C_{cavity} determines the extent of acoustic leakage. The cutoff frequency is typically defined at the −3 dB point, as shown in Eq. (6). For acoustic applications, a stricter definition is appropriate since human hearing can discriminate intensity changes of about 1 dB [20]. The corresponding cutoff frequency for −1 dB is given in Eq. (7).

$$|H(f)| = \frac{1}{\sqrt{1 + \left(\frac{1}{2\pi \cdot f \cdot R_{\text{slit}} \cdot C_{\text{cavity}}}\right)^2}} \tag{5}$$

$$f_{\text{c}} = \frac{1}{2\pi \cdot R_{\text{slit}} \cdot C_{\text{cavity}}} \tag{6}$$

$$f_{\text{c}_{1\,\text{dB}}} = \frac{f_{\text{c}}}{\sqrt{\frac{1}{\left(10^{\frac{-1dB}{20}}\right)^2} - 1}} \approx 1.965 \cdot f_{\text{c}} \tag{7}$$

3.3. Verification with FEM

To validate the analytical model, two-dimensional FEM simulations were conducted in COMSOL Multiphysics using thermoviscous acoustics. A slit depth of $b = 1$ m was chosen to ensure that $b \gg d$, eliminating the need for a resistance correction factor. However, these simulations also highlight the physical limitations of the analytical approach. Although a Hagen-Poiseuille flow profile forms, the analytical and FEM results agree within 10 % only when the slit length-to-width ratio is below 1.25, as the analytical formula assumes a long and narrow slit.

Further limitations arise from the fluid flow regime, characterized by the Knudsen number $Kn = \frac{\lambda}{L_{\text{K}}}$, where λ denotes the mean free path of the gas particles and L_{K} represents the characteristic device length [18]. For $Kn \leq 0.01$, the flow remains in the continuum regime, where the Navier-Stokes equations are applicable. In contrast, for $0.01 \leq Kn \leq 0.1$, the interaction between the fluid particles and the channel walls decreases, leading to velocity slip. Since the analytical model neglects these effects, it loses its validity in the slip regime where slit dimensions are below 6.5 µm and thus serves only as an approximation for certain MEMS speaker dimensions.

The FEM model comprises a cavity representing the ear coupler volume and a moving plate with a central slit that compresses the air inside. As shown in Fig. 2, the acoustic velocity in the slit exhibits a characteristic Hagen-Poiseuille flow profile. Opposite the cavity, the plate borders an air domain terminated by a perfectly matched layer. The plate is driven by a frequency-dependent velocity boundary condition, representing a movement with constant displacement.

The transfer function in the FEM model is calculated by dividing the pressure in the cavity by the linearized adiabatic equation, as shown in Eq. (8), where $\hat{V}$ is the amplitude of cavity volume change.

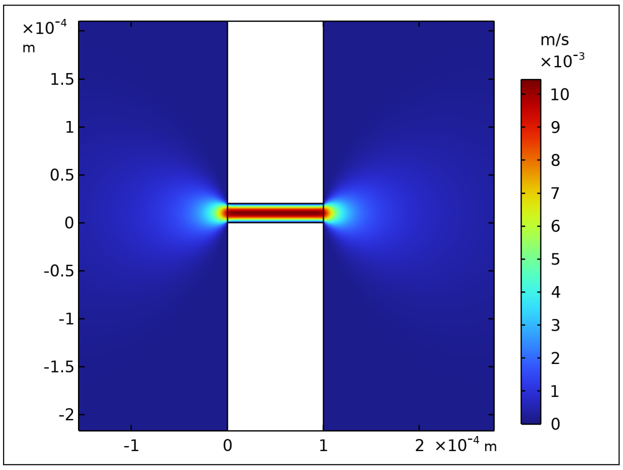

Figure 2: Acoustic velocity profile in the model to simulate slit leakage.

$$|H(f)| = \frac{p_{\text{cavity}} \cdot V_0}{\kappa \cdot p_0 \cdot \hat{V}} \tag{8}$$

The analytical and FEM transfer functions both show a high-pass filter response, as shown in Fig. 3. Agreement between both approaches depends on slit geometry. For an error below 10 %, the slit length l must be at least ten times the slit width d. Furthermore, the analytical model does not account for the resistance of the opening areas.

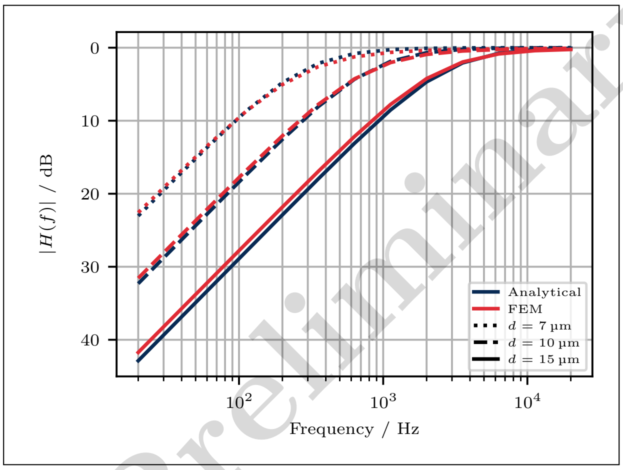

Figure 3: Comparison of analytical to FEM transfer function with depth of $b = 1$ m and slit length of $l = 100$ µm.

3.4. Numerical Validation of Slit Dimension Criteria

For typical MEMS speaker dimensions, as described in our previous work [8], a moving plate area of 10 mm^2, resulting in a depth of $b = \sqrt{10}$ mm are used. Simulations were performed for slit widths d of 7 and 10 µm and slit lengths l of 10 and 15 µm. FEM analysis is necessary because the slit depth is comparable to the slit width. The slit width is kept above 7 µm to ensure continuum flow regime with no-slip boundary conditions.

The results for these parameters are shown in Fig. 4. For a slit width of $d = 7$ µm, the cutoff at -1 dB is nearly reached at 20 Hz. This confirms that, for typical MEMS speaker dimensions, leakage can be suppressed by slit widths of about 5 µm. However, this may not apply to all possible parameter variations.

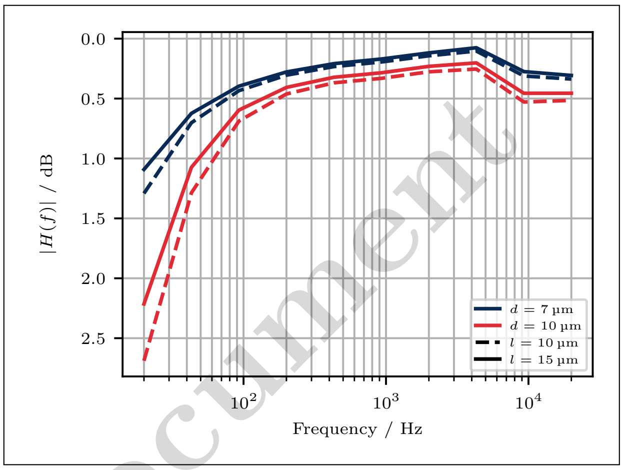

Figure 4: FEM transfer functions for typical dimensions of MEMS speakers validating sufficient sealing with slit width $d < 5$ µm.

The increased leakage observed at higher frequencies in Fig. 4 may be related to resonance effects in the cavity, which was modeled as a rectangular volume.

4. Conclusion

According to the available literature, sealing improves low-frequency performance compared to unsealed designs. The MOAC approach is most effective when slit widths are below 5 µm, allowing the device to function as intended without added manufacturing or structural complexity. If this is not feasible, sealing with PDMS is preferred, as it preserves the frequency response due to its low Young's modulus compared to Parylene-C. Although sealing increases fabrication complexity, it can enhance robustness against moisture, dust, and mechanical stress.

The proposed analytical model and the criterion for leakage have been verified with FEM simulations, showing good agreement for typical MEMS speaker dimensions. Further investigation is needed for the slip flow regime and for higher frequencies relevant to ultrasound pulse-based speakers.

Depending on the diaphragm structure, sealing strategy, and materials, sealing can also have adverse effects on the frequency response. Therefore, it is advised to decide for the sealing strategy early in the design process, especially considering the available manufacturing capabilities and robustness requirements.

5. Acknowledgments

The IPCEI ME/CT project is supported by the Federal Ministry for Economic Affairs and Climate Action on the basis of a decision by the German Parliament, by the Ministry for Economic Affairs, Labor and Tourism of Baden-Württemberg based on a decision of the State Parliament of Baden-Württemberg, the Free State of Saxony on the basis of the budget adopted by the Saxon State Parliament, the Bavarian State Ministry for Economic Affairs, Regional Development and Energy, and funded by the European Union – NextGenerationEU.

References

[1] C. Gazzola et al., "On the Design and Modeling of a Full-Range Piezoelectric MEMS Loudspeaker for In-Ear Applications," *Journal of Microelectromechanical Systems*, vol. 32, no. 6, pp. 626–637, 2023. DOI: 10.1109/JMEMS.2023.3312254.

[2] Q. Wang et al., "Obtaining High SPL Piezoelectric MEMS Speaker via a Rigid-Flexible Vibration Coupling Mechanism," *Journal of Microelectromechanical Systems*, vol. 30, no. 5, pp. 725–732, 2021. DOI: 10.1109/JMEMS.2021.3087718.

[3] Y. Lang et al., "Piezoelectric bimorph MEMS speakers," *Nanotechnology and Precision Engineering*, vol. 5, no. 3, p. 033 001, 2022. DOI: 10.1063/10.0013406.

[4] F. Stoppel et al., "Highly miniaturized 115 dB full-range MEMS loudspeaker for in-ear applications," *Sensors and Actuators A: Physical*, vol. 387, p. 116 373, 2025. DOI: 10.1016/j.sna.2025.116373.

[5] F. Stoppel et al., "Novel membrane-less two-way MEMS loudspeaker based on piezoelectric dual-concentric actuators," in *IEEE TRANSDUCERS*, 2017, pp. 2047–2050. DOI: 10.1109/TRANSDUCERS.2017.7994475.

[6] Y. Ma et al., "A PZT MEMS loudspeaker with a quasi-closed diaphragm," *Sensors and Actuators A: Physical*, vol. 358, p. 114 454, 2023. DOI: 10.1016/j.sna.2023.114454.

[7] L. Xu et al., "A Piezoelectric MEMS Speaker with Stretchable Film Sealing," in *IEEE MEMS*, 2023, pp. 673–676. DOI: 10.1109/MEMS49605.2023.10052314.

[8] N. Wittek, A. Melnikov, B. Kaiser, and A. Zimmermann, "Review of MEMS speakers for audio applications," 2025. DOI: 10.48550/ARXIV.2512.17708.

[9] F. Stoppel et al., "New integrated full-range MEMS speaker for in-ear applications," in *IEEE MEMS*, 2018, pp. 1068–1071. DOI: 10.1109/MEMSYS.2018.8346744.

[10] F. Cerini et al., "High-Performance Piezoelectric MEMS Speakers for in-ear Applications," in *IEEE Transducers*, 2025, pp. 443–446. DOI: 10.1109/Transducers61432.2025.11111254.

[11] N. Deng et al., "Optimization of Dual-electrode Ratio and Driving Phase of Piezoelectric MEMS Speakers for Improving Sound Pressure Level," *Sensors and Actuators A: Physical*, pp. 116 109–116 109, 2024. DOI: 10.1016/J.SNA.2024.116109.

[12] Q. Wang, Z. Hu, T. Ruan, and J. Zhao, "Unsealed piezoelectric MEMS speaker with rigid-flexible composite membrane," *Journal of Micromechanics and Microengineering*, vol. 34, no. 6, p. 065 003, 2024. DOI: 10.1088/1361-6439/ad42a6.

[13] Y. Wang, T. Lv, J. Zhang, and H. Yu, "Capillary effect-based selective sealing strategy for increasing piezoelectric MEMS speaker performance," *Microsystems & Nanoengineering*, vol. 10, no. 1, pp. 1–13, 2024. DOI: 10.1038/s41378-024-00753-x.

[14] P. Chen, T. Lv, Y. Wang, J. Zhang, and H. Yu, "Monolithic frequency superposition Scandium-doped Aluminum Nitride based piezoelectric MEMS speaker with user-defined boundary," *Sensors and Actuators A: Physical*, vol. 387, p. 116 375, 2025. DOI: 10.1016/j.sna.2025.116375.

[15] Q. Zheng et al., "An Ultra-High Low-Frequency SPL Piezoelectric MEMS Loudspeaker Based on Sputtered PZT," *Sensors and Actuators A: Physical*, p. 116 551, 2025. DOI: 10.1016/j.sna.2025.116551.

[16] Q. Zheng et al., "A High-SPL Full-Range PZT MEMS Speaker for In-Ear Applications," *IEEE Transactions on Electron Devices*, pp. 1–10, 2025. DOI: 10.1109/TED.2025.3579682.

[17] A. Lenk, R. G. Ballas, R. Werthschützky, and G. Pfeifer, *Electromechanical Systems in Microtechnology and Mechatronics*. Springer Berlin Heidelberg, 2011. DOI: 10.1007/978-3-642-10806-8.

[18] V. Kempe, *Inertial MEMS: principles and practice*. Cambridge University Press, 2011, ISBN: 978-0-521-76658-6.

[19] J. Borwick, Ed., *Loud speaker and headphone handbook*, 3rd ed. Focal Press, 2001, ISBN: 978-0-240-51578-6.

[20] T. D. Rossing, Ed., *Springer Handbook of Acoustics*. Springer New York, 2014. DOI: 10.1007/978-1-4939-0755-7.